Modulating spin transfer torque switching dynamics with two orthogonal spin-polarizers by varying the cell aspect ratio

B. Lacoste,[1] M. Marins de Castro,[1] T. Devolder,[2] R. C. Sousa,[1] L. D. Buda-Prejbeanu,[1] S. Auffret,[1] U. Ebels,[1] C. Ducruet,[3] I. L. Prejbeanu,[3] L. Vila,[4] B. Rodmacq,[1] and B. Dieny[1]

[1]*SPINTEC, UMR CEA/CNRS/UJF-Grenoble 1/ Grenoble-INP, INAC, F-38054 Grenoble, France*

[2]*Institut d'Electronique Fondamentale, CNRS UMR 8622, Bat. 220, Université Paris-Sud, 91405 Orsay, France*

[3]*Crocus Technology, 38025 Grenoble, France*

[4]*SP2M/NM, CEA/Grenoble, INAC, 38054 Grenoble Cedex, France*

(Received 6 May 2014; revised manuscript received 20 November 2014; published 1 December 2014)

We study in-plane magnetic tunnel junctions with additional perpendicular polarizer for subnanosecond-current-induced switching memories. The spin-transfer-torque switching dynamics was studied as a function of the cell aspect ratio both experimentally and by numerical simulations using the macrospin model. We show that the anisotropy field plays a significant role in the dynamics, along with the relative amplitude of the two spin-torque contributions. This was confirmed by micromagnetic simulations. Real-time measurements of the reversal were performed with samples of low and high aspect ratio. For low aspect ratios, a precessional motion of the magnetization was observed and the effect of temperature on the precession coherence was studied. For high aspect ratios, we observed magnetization reversals in less than 1 ns for high enough current densities, the final state being controlled by the current direction in the magnetic tunnel junction cell.

DOI: 10.1103/PhysRevB.90.224404 PACS number(s): 85.70.Kh, 75.70.Cn, 75.78.−n, 85.75.−d

Spin transfer torque (STT) magnetic random-access memory (MRAM) are very promising nonvolatile memories envisioned to provide devices of smaller sizes and faster dynamics. A conventional STT-MRAM consists of a reference layer, whose magnetization is fixed either in-plane or out-of-plane, separated by an MgO barrier from the storage layer (SL), whose magnetization is free. The SL magnetization has two stable configurations, parallel (P) and antiparallel (AP) to the reference layer. To write the memory cell, a voltage pulse is applied to the magnetic tunnel junction (MTJ) that can reverse the SL magnetization, thanks to the STT of the polarized current due to the reference layer. However the STT is proportional to the vectorial product of the reference-layer magnetization and the SL magnetization, so that, in the equilibrium configuration (P or AP), the STT vanishes. The reversal of the MTJ is only possible thanks to thermal fluctuations that misalign the two layer magnetizations, resulting in a stochastic switching dynamics in conventional STT-MRAM. In fact, even if the switching itself lasts less than a nanosecond, the switching occurs after a random incubation time. This is detrimental to the switching time, as it is difficult to switch an MTJ with a bit error rate lower than 10^{-4} in less than 10 ns [1,2], which is necessary for application as a fast RAM.

In order to eliminate the incubation time, it was proposed to add another polarizing layer with a magnetization fixed and orthogonal to the equilibrium directions of the SL magnetization, in order to maximize the STT acting on the SL magnetization as soon as the write current pulse is switched on, while the SL magnetization is still aligned along its equilibrium direction [3–6]. Switching times <1 ns were observed with this design [7]. The same configuration is studied here. The in-plane SL is separated from the in-plane reference layer by an MgO barrier, compared to previous work with a spin valve [8], to improve the STT from the reference layer and to obtain an output signal large enough for time-resolved measurements. An additional perpendicular polarizer (PP), whose magnetization is out-of-plane, is separated from the SL by a nonmagnetic spacer. Although it was previously observed that the presence of the PP reduces switching times, the magnetization dynamics with two polarizing layers is not completely understood, especially the relative influence of the two polarizers. Here we propose a theoretical model, confirmed experimentally, to describe the crossover between precessional motion of the SL magnetization and switching with two polarizers, due to a change in the anisotropy field.

With this geometry, described in Fig. 1(a), the SL magnetization is submitted to two STT contributions, which have different effects on the SL magnetization dynamics. Note that this analysis can be applied to the modeling of a free layer with spin-orbit torque in an arbitrary direction, because the macrospin equation is similar [9], or for an out-of-plane MTJ with an additional in-plane polarizer. In the following, M_s is the saturation magnetization of the SL, H_K the in-plane anisotropy field, M_{eff} the reduced demagnetizing field (due to interface perpendicular anisotropy, for instance), t the thickness of the SL, α the Gilbert damping constant, and η_{LONG} and η_{PERP} the STT efficiency of the reference layer and of the PP, respectively.

On the one hand, the STT contribution from the PP pulls the SL magnetization out-of-plane [Fig. 1(b)], then due to the strong demagnetizing field, the FL magnetization precesses around the out-of-plane axis at a gigahertz frequency. The free-layer magnetization is in out-of-plane precession (OPP) around the z axis when a current density higher than the critical current density J_c^{PERP} [10,11] is applied:

$$J_c^{\text{PERP}} = \frac{2e}{\hbar}\frac{\mu_0 M_s t}{\eta_{\text{PERP}}}\frac{H_K}{2}. \quad (1)$$

By tailoring the current pulse width, it is possible to stop the FL magnetization precession after half a precession, hence reversing the magnetization direction and switching the device [5,6]. However, achieving a 180° SL magnetization

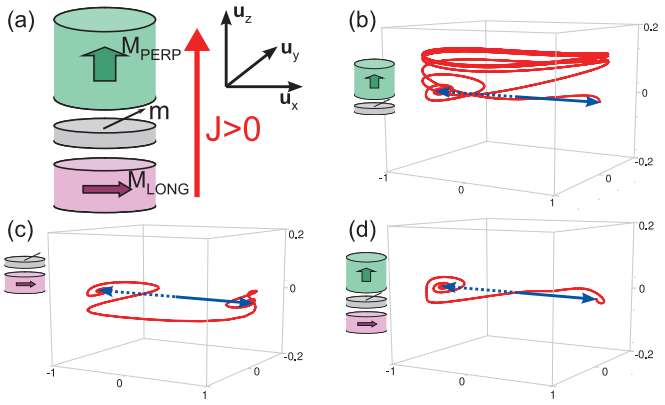

FIG. 1. (Color online) (a) Geometry of a nanopillar with an elliptical cross section. (b)–(d) Magnetization dynamics during the reversal of the storage layer in three configurations: (b) with a perpendicular polarizer only, (c) with an in-plane reference layer only, and (d) with both polarizing layers. The magnetization is initially in the parallel configuration [solid (blue) arrow] and relaxes in the antiparallel state [dotted (blue) arrow].

rotation implies being able to control the pulse duration with a typical accuracy of 200 ± 50 ps [12]. This is possible at the single-cell level but much more difficult at a memory chip level due to the deformation of the current pulses during their propagation along the bit lines. Furthermore, since this write procedure is similar to a toggle writing, it requires reading before writing.

On the other hand, the STT contribution from the analyzer provokes a bipolar switching of the FL magnetization [Fig. 1(c)]. The expression of the critical current density J_c^{LONG} comes from the study of the equilibrium stability [13–15]:

$$J_c^{\mathrm{LONG}} = \frac{2e}{\hbar}\frac{\mu_0 M_s t}{\eta_{\mathrm{LONG}}}\alpha\left(\frac{M_{\mathrm{eff}}}{2} + H_K\right). \tag{2}$$

Depending on the polarity of the current, one of the two stable configurations, P or AP, is favored, so that the final written state can be controlled by the current direction. However, the switching is then stochastic as previously explained.

By combining the two STT contributions from the two orthogonal polarizing layers, one can expect to be able still to control the final state by the current pulse direction through the MTJ while reducing the stochasticity of the switching thanks to the STT contribution from the PP [Fig. 1(d)]. But this requires proper tuning of the relative amplitude of these two STT contributions [7,16–19].

However, from the expressions of the two critical currents, it appears that if the uniaxial anisotropy field H_K is increased, the critical current that controls the appearance of the precessional motion is also increased [Eq. (1)], while the critical current for bipolar switching is not changed much because $H_K \ll M_{\mathrm{eff}}$ for in-plane MTJ. Hence, instead of tuning the relative amplitude of the two STT contributions, this qualitative analysis suggests increasing the anisotropy field H_K to favor bipolar switching over the precessional regime.

If the two STT contributions of the reference layer and of the PP are included in the Landau-Lifshitz-Gilbert-Slonczewski (LLGS) equation that describes the dynamics of the free layer, the equilibrium analysis in the macrospin approximation exhibits two critical current densities, whose values are close to J_c^{LONG} and J_c^{PERP}. A more extended calculation of the critical currents is presented in the Appendix. In a nutshell, below J_c^{LONG}, the magnetization remains in equilibrium. And above J_c^{PERP}, only the dynamic OPP state exists. However, between these two current densities, both the OPP and the switched state can be reached. However, the critical current J_c^{OPP} below which the OPP state cannot exist was computed by studying the stability of the OPP with an anisotropy field and the STT from the reference layer [20]:

$$J_c^{\mathrm{OP}} = \frac{2e}{\hbar}\frac{\mu_0 M_s t}{\eta_{\mathrm{PERP}}}\frac{\alpha}{2}\sqrt{H_K M_{\mathrm{eff}}}. \tag{3}$$

This critical current depends on the anisotropy field H_K, but because of the square root dependence it is smaller than J_c^{PERP}. Between these two critical current densities, the magnetization can be in two bistable states: the OPP and the switched state. The final state depends on the detail of the dynamics.

To describe the bistable region AP/OPP and to validate the critical line expressions, we performed macrospin simulations with different anisotropy fields H_k and polarizations of the PP η_{PERP}. The parameters for the simulations are $\alpha = 0.02$, $t = 3$ nm, $M_S = M_{\mathrm{eff}} = 1.2\times10^6$ A/m, $\eta_{\mathrm{LONG}} = 0.3$, and a magnetization initially in the P state ($m_x = 1$). The average in-plane magnetization component m_x in the permanent regime is calculated for different values of the applied current density J_{app} and polarization η_{PERP} and is represented in Fig. 2(a) at $H_k = 6$ kA/m and Fig. 2(b) at $H_k = 24$ kA/m. The diagrams show three regions: (i) In the red area, the final state remains the initial P state, and the SL has not switched. (ii) In the blue region, the final state is the AP state, and the SL has switched. (iii) In the green area, the SL is in OPP steady state, and the final state depends on the current density pulse duration. The analytical critical line for reversal (dotted black line) is in agreement with the macrospin simulations. However, the border between the OPP (green) region and the switching (blue) region does not correspond to any theoretical critical line, as it stands in the bistable region delimited by the dashed black line, for the appearance of OPP and the dash-dotted (green) line, for the disappearance of OPP. Note that for negative current densities, the dashed black critical line is in agreement with the simulations, because the initial P equilibrium is stable until this critical line. The effect of the anisotropy field was confirmed by the simulations: If the anisotropy field is increased, the range of bipolar switching (blue region) is increased, at the expense of the OPP (red) region.

We also confirmed the impact of the anisotropy on the reversal with micromagnetic simulations with two polarizing layers. The final state after 10 ns is represented by the symbols in in Fig. 2. The micromagnetic simulations were carried out on a cylindrical free layer with an elliptical section of dimensions $105\times95\times3$ nm, which corresponds to $H_k = 6$ kA/m, and $180\times60\times3$ nm, which corresponds to $H_k = 24$ kA/m. The exchange stiffness constant was set to 1.6×10^{-11} J/m, all the other parameters being the same as for the macrospin simulations.

In Fig. 2, the boundary for the stability of the initial P configuration is similar in micromagnetics as that in the

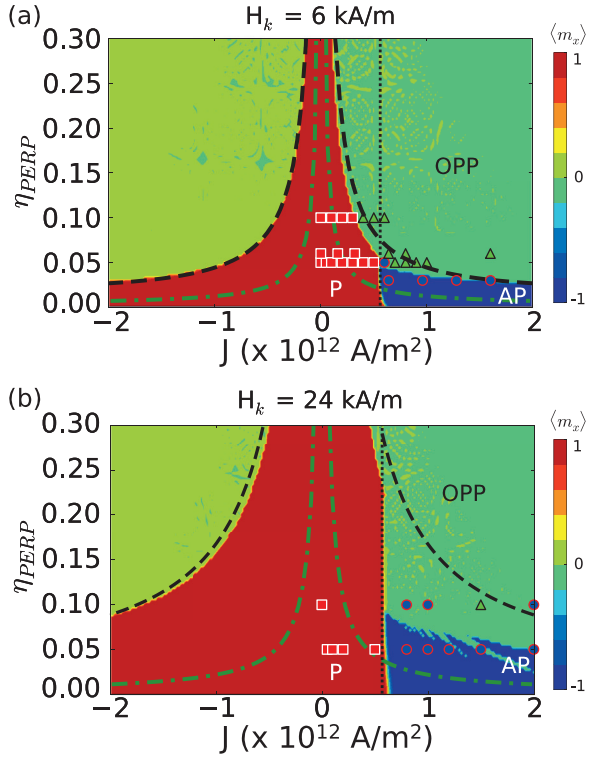

FIG. 2. (Color online) Macrospin simulation of the average in-plane magnetization m_x versus the current density and polarization of the perpendicular polarizer, with $\eta_{\mathrm{LONG}} = 0.3$, for different anisotropy fields: (a) 6 kA/m and (b) 24 kA/m. There are three final steady states: (i) red region, the P final state, with no switching; (ii) blue region, the AP final state, with switching of the SL magnetization; and (iii) green region, where the average in-plane component of the magnetization vanishes, corresponding to an OPP steady state. Right of the dotted black-line the P equilibrium is unstable. Above the dashed black line, only OPP exists. Below the dash-dotted (green) line OPP cannot exist. Symbols represent the final steady state from micromagnetic simulations: P final state [(orange) squares], AP final state [(blue) circles], and OPP [(green) triangles].

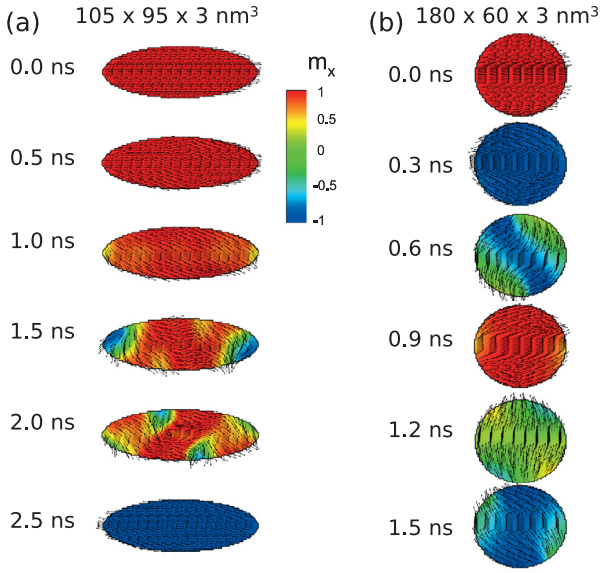

FIG. 3. (Color online) Snapshots of the micromagnetic configuration of the free layer at different times for (a) the high aspect ratio of 180×60×3 nm and (b) the low aspect ratio of 105×95×3 nm. The spin polarization of the reference layer and the perpendicular polarizer are $\eta_{\mathrm{LONG}} = 0.3$ and $\eta_{\mathrm{PERP}} = 0.05$, respectively. The current density is 10^{12} A/m^2.

macrospin model: the orange squares, which stand for a final P state that is not reversed, are situated in the P region. This is due to the fact that the initial micromagnetic configuration is uniformly magnetized, except at the edges, very similarly to the macrospin approximation. However, the boundary between the reversal and the precessional state differs in micromagnetic simulations. It appears that the OPP state is less stable in micromagnetics, mainly because the precession is not spatially uniform, so the macrospin picture is not valid anymore. As a result, in the bistable AP/OPP region, some set of parameters for which a final OPP state was observed in macrospin appears to be reversals in micromagnetic simulations. For high current densities and large PP spin polarization η_{PERP}, though, a nonuniform, high-amplitude, out-of-plane precessional motion was observed, in agreement with the macrospin analysis.

As for the effect of the aspect ratio, the trend is the same as predicted by the macrospin simulations; a higher aspect ratio favors switching. Figure 3 shows snapshots of the micromagnetic configuration at different times for a high aspect ratio and a low aspect ratio, with a current density of 10^{12} A/m^2. For a high aspect ratio, a reversal of the free-layer magnetization is observed, whereas for a low aspect ratio, with the other parameters kept unchanged, we found a high-amplitude-oscillation dynamical state. This is in agreement with the macrospin study.

In order to demonstrate the impact of the aspect ratio, in-plane MTJ stacks with PP were grown and patterned with different aspect ratios. Real-time measurements of the resistance change were then performed on these samples submitted to voltage pulses. The stacks are described in Ref. [5]. They consist of, from bottom to top: a synthetic antiferromagnet PP/3 nm Cu spacer/free (storage) layer/MgO barrier/reference layer. The PP is a synthetic antiferromagnetic multilayer of composition (in nm) Ta 3/Pt 5/[Co 0.5/Pt 0.4] × 5/Co 0.5/Ru 0.9/[Co 0.5/Pt 0.4] × 3/Co 0.5/CoFeB 1. The free layer is also a synthetic antiferromagnetic stack consisting of (in nm) CoFeB 1.3/Ru 0.9/CoFeB 1.7. The reference layer is made of (in nm) CoFeB 3/Ru 0.9/Co 2/IrMn 7. The MgO barrier between the storage and reference layer is realized by, first, deposition of Mg and, then, a 10-s natural oxidation under a 160-mb oxygen pressure.

All the layers are synthetic antiferromagnets, to minimize their mutual magnetostatic interactions. After deposition, the samples were annealed at 300°C for 90 min under an in-plane magnetic field of 0.23 T. Then the sample was patterned in elliptical nanopillars of various aspect ratios. We measured an average TMR signal of about 70% and an $R \times A$ product of 17 $\Omega \cdot \mu$m^2. Due to a residual stray field, the AP alignment is favored in the samples.

The nanopillars are connected to a resistance-versus-field measurement bench. On top of this setup, at any given field,

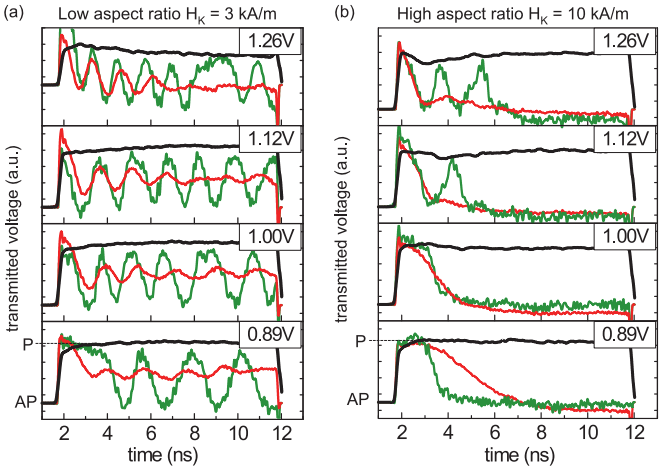

FIG. 4. (Color online) Transmitted voltage with an applied voltage pulse of 0.89, 1.00, 1.12, and 1.26 V (from bottom to top) in an MTJ nanopillar with (a) a low aspect ratio and (b) a high aspect ratio. The MTJ is initially in the P state. Black line, reference resistance in the AP state taken with an external field to saturate the junction. Green line, a single-shot trace. Red line, average of 50 traces.

it is possible to send a voltage pulse of 10-ns width through the nanopillar and measure the transmitted voltage with an oscilloscope in real time [1]. An external bias field is applied to compensate for the residual stray field on the SL.

The switching probabilities versus pulse durations were also measured, by measuring the resistance after the current pulse application and comparing it with the resistance before. These measurements were averaged over 100 hysteresis curves, by sending the pulse in the center of the hysteresis loop and for different pulse widths, ranging from 100 ps to 10 ns.

First, we focus on samples with the low aspect ratio of 2.5:1, with nominal sizes of 170×70×3 nm. The in-plane anisotropy field is measured to be around 3 kA/m. In these samples the effect of the PP is dominant, so a precessional motion of the SL magnetization around the out-of-plane axis is expected. Figure 4(a) shows the transmitted voltage during a pulse of 10 ns and of different voltages (0.89, 1.0, 1.12, and 1.26 V) through the MTJ. In these voltage ranges, the magnetoresistance (green curve) oscillates between the two values corresponding to P and AP resistance (black reference curve). This high-amplitude oscillation is characteristic of the action of the PP. As shown in Fig. 5(a), the precession is not coherent because of thermal fluctuations, the frequency is not well defined, and the single-shot signals exhibit phase noise. This decoherence is responsible for the decay of the average of 50 traces, the red curves in Fig. 4. We also observe damped oscillations of the switching probability with the pulse width, as shown in Fig. 5(b), with a decay due to the thermal fluctuations. The characteristic time of the decay is around 10 ns, which is consistent with the inverse linewidth observed in spin-torque oscillators with a PP (∼100 MHz) [8].

Real-time measurements on a low-aspect-ratio sample were performed at different temperatures from 80 to 400 K. Typical single-shot traces of the transmitted voltage at different temperatures are presented in Fig. 6(a). They show that the

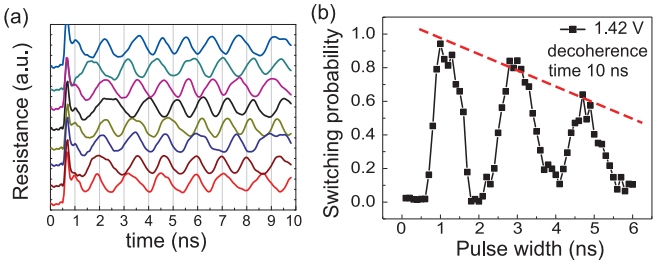

FIG. 5. (Color online) Low-aspect-ratio MTJ at room temperature. (a) Single-shot traces for the same applied voltage pulse of 1.42 V. A low-pass filter at 3 GHz was applied. (b) Switching probability of an MTJ initially in the P state versus the applied pulse width, with the voltage amplitude set to 1.42 V. Dashed (red) line: oscillation decay.

precession phase and amplitude are more stable at low temperatures (80 K). Due to thermal fluctuations, some precessions are missing above 240 K. The precession frequency was found to be proportional to the applied voltage of the pulse, in agreement with OPP spin-torque oscillators [8]. While considering the large uncertainty in the measured frequency, the proportionality factor seems to be the same for each temperature. In the macrospin model the OPP frequency is given by [10]

$$f = \frac{\gamma}{2\pi\alpha}\frac{\hbar}{2e}\frac{\eta_{\mathrm{PERP}}}{M_s t}J. \tag{4}$$

Given that η_{PERP} and M_s depend on the temperature, this result seems to indicate that the thermal dependence of the STT efficiency (spin polarization) and saturation magnetization are similar, which sounds reasonable. However, micromagnetic simulations show that the free layer is not uniformly magnetized in the OPP state, therefore the macrospin model is not totally adapted to describe the OPP and caution should be taken when using the formula for the frequency.

We next measured samples with the higher aspect ratio of 3.7:1, with nominal sizes of 260×70×3 nm. The in-plane anisotropy field is measured to be around 10 kA/m.

The real-time transmitted voltage for different applied pulse amplitudes (0.89, 1.0, 1.12, and 1.26 V) is displayed in Fig. 4(b). The MTJ is initially in the P state. As expected

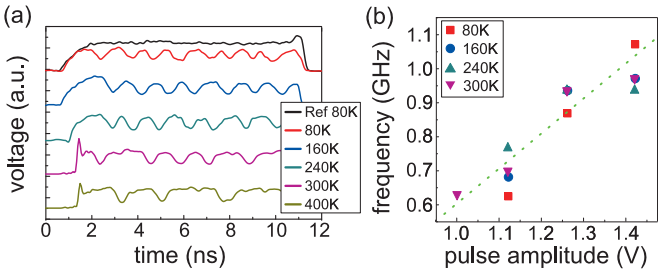

FIG. 6. (Color online) Low-aspect-ratio MTJ. (a) Single-shot transmitted voltage with a pulse of 1.26 V at different temperatures (from top to bottom): 80, 160, 240, 300, and 400 K. The P reference voltage is shown at 80 K (black line). (b) Oscillation frequency versus applied voltage pulse at different temperatures. The dependency is almost linear.

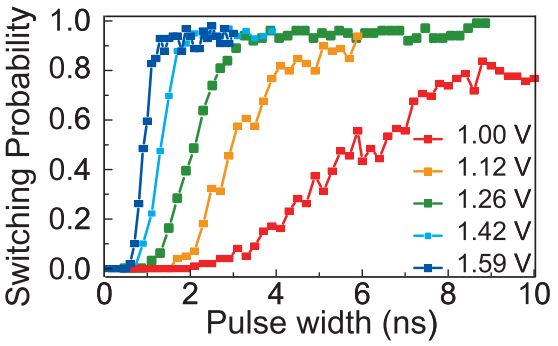

FIG. 7. (Color online) High-aspect-ratio MTJ. Switching probability of an MTJ initially in the P state versus applied voltage pulse width. The pulse amplitude varies from 1.0 to 1.59 V.

from the simulations, close to the critical current density, no precessional motion of the magnetoresistance was observed; only a reversal of the SL magnetization. Such time-resolved measurements of MTJs with an orthogonal polarizer have never been realized before and should be compared to similar switching measurements on MTJs without a PP [1], in particular, regarding the incubation time, which vanishes with the PP. When the applied pulse voltage is increased, the switching time is decreased, as with a MTJ without a PP. At higher voltages, hints of precessional motion begin tot appear. This was expected from simulations: For a given spin polarization of the PP η_{PERP}, the magnetization enters into precession for high applied current densities, above the current density range for reversal. This back-hopping could be reduced or even suppressed by reducing the spin polarization of the PP below the range of the appearance of OPP (see Fig. 2 and the Appendix).

Figure 7 shows the switching probability versus the pulse width for different voltage pulse amplitudes in the case of cells with a high aspect ratio. In contrast to the low-aspect-ratio case [Fig. 5(b)], no oscillations are observed in the switching probability. For sufficiently long pulses, the final state is fully controlled by the current direction independently of the pulse duration. Furthermore, the higher the pulse amplitude, the faster the switching. Subnanosecond switching was observed for a pulse amplitude above 1.12 V, which corresponds to a current density of 6×10^{11} A/m^2 and a switching energy of around 1.5 pJ. This is comparable to, although larger than, the values obtained previously with optimized stacks [7].

The integration of a PP with an in-plane MTJ permitted us to realize a subnanosecond bipolar reversal of the SL magnetization. For practical devices, the STT contributions from the in-plane analyzer and PP must be tuned so that the PP can still provide the initial impulse which reduces the stochasticity of the switching, but the final state is controlled by the current direction in the stack independently of the pulse duration. This can be achieved by increasing the aspect ratio of the cell above ~3. This also improves the thermal stability of the cell. The drawback is the increased footprint of the cell, but conventional CMOS SRAMs have large footprints anyway. Therefore, these high-anisotropy structures with orthogonal polarizers are good candidates for realizing ultrafast MRAM for SRAM types of applications.

ACKNOWLEDGMENT

This work was supported by the European Research Council through the Advanced Grant HYMAGINE (ERC No. 246942).

APPENDIX: EQUILIBRIUM STABILITY

The equilibrium states of the free-layer magnetization $\mathbf{m} = (m_x, m_y, m_z)$ are computed from the LLGS equation including the STT contributions from the two polarizing layers [20], the in-plane reference layer and the PP. The equilibrium in-plane and out-of-plane angles are noted ϕ and θ:

$$m_x = \sin\theta\cos\phi, \quad m_y = \sin\theta\sin\phi, \quad m_z = \cos\theta.$$

The equilibrium angles are solutions of the LLGS equation with the time-dependent terms set to 0:

$$0 = -\frac{H_K}{2}\sin\theta\sin(2\phi) - P_z\sin\theta - P_x\cos\theta\cos\phi,$$
$$0 = -\sin\theta\cos\theta(M_{\mathrm{eff}} + H_K\cos^2\phi) + P_x\sin\phi. \quad \text{(A1)}$$

M_{eff} is the reduced demagnetizing field, H_K is the in-plane anisotropy field, and P_x and P_z are the spin-torque amplitudes due to the reference layer (magnetized along the x axis) and the PP, respectively. Their expressions are given by

$$P_{x(z)} = \frac{\hbar}{2e}\frac{\eta_{\mathrm{LONG(PERP)}}}{\mu_0 M_s t}J.$$

M_s is the saturation magnetization of the SL; J, the applied current density; t, the thickness of the SL; and η_{LONG} and η_{PERP}, the STT efficiencies of the reference layer and of the PP.

The expression of the out-of-plane angle θ at equilibrium with respect to the angle ϕ is computed from the second Eq. (A1):

$$\sin(2\theta) = \frac{2P_x\sin\phi}{M_{\mathrm{eff}} + H_K\cos^2\phi}. \quad \text{(A2)}$$

For clarity, let $A = \frac{2P_x\sin\phi}{M_{\mathrm{eff}}+H_K\cos^2\phi}$. We make the assumption that the demagnetizing field is dominant, so $A^2 \ll 1$. From Eq. (A2), the two possible values of the cotangent of θ are given by

$$\cot(\theta)_\pm = \frac{1}{A}(1 \pm \sqrt{1-A^2}).$$

The two solutions describe an in-plane (IPS) equilibrium and an out-of-plane equilibrium (OPS), for which $\cos\theta \approx A/2$ and $\sin\theta \approx A/2$, respectively. Replacing $\cos\theta$ and $\sin\theta$ in the first Eq. (A1), the expression of the in-plane angle ϕ at equilibrium is obtained for the IPS and OPS equilibriums.

$$\text{OPS:} \quad \cot\phi = \frac{-P_z}{M_{\mathrm{eff}} + H_K}. \quad \text{(A3)}$$

$$\text{IPS:} \quad \sin(2\phi) = \frac{-2P_z}{H_K + \frac{P_x^2}{M_{\mathrm{eff}}+H_K/2}}. \quad \text{(A4)}$$

The OPS equilibrium is always defined. However, the IPS equilibrium is defined only if the right-hand side of the previous expression of ϕ is smaller than unity in absolute

value, i.e.,

$$2|P_z| < H_K + \frac{P_x^2}{M_{\text{eff}} + H_K/2}. \tag{A5}$$

Let $k_0 = \frac{2e}{\hbar}\mu_0 M_s t$; from the expressions of P_x and P_z, the criterion for the existence of an IPS equilibrium becomes

$$\eta_{\text{PERP}} < \frac{H_K k_0}{2J} + \frac{\eta_{\text{LONG}}^2 J}{2k_0(M_{\text{eff}} + H_K/2)}. \tag{A6}$$

For the range of applied current densities used in applications, the second term in Eq. (A6) is negligible, so the range of current densities for which the magnetization of the free layer is in OPP (because no IPS equilibrium exists and the OPS equilibrium is unstable) corresponds to current densities higher than J_c^{PERP}.

It is interesting to note that the left-hand side of Eq. (A6) goes through a minimum when the current is changing. This gives rise to a maximum for η_{PERP} below which the IPS equilibrium exists for all applied current densities J, so OPP is not expected for any current density. The maximum of η_{PERP} is given by

$$\eta_{\text{PERP}}^{\max} = \eta_{\text{LONG}}\sqrt{\frac{H_K}{M_{\text{eff}} + H_K/2}}.$$

After studying the existence of the equilibrium, one must look at their stability by linearizing the LLGS equation. After simplification with the assumption that M_{eff} is the dominant field, we find that, for reasonable current densities, the initial equilibrium-state IPS is destabilized for applied current densities above the critical current density J_c^{LONG}.

[1] T. Devolder, J. Hayakawa, K. Ito, H. Takahashi, S. Ikeda, P. Crozat, N. Zerounian, J.-V. Kim, C. Chappert, and H. Ohno, Phys. Rev. Lett. **100**, 057206 (2008).

[2] R. Koch, J. Katine, and J. Sun, Phys. Rev. Lett. **92**, 088302 (2004).

[3] O. Redon, B. Dieny, and B. Rodmacq, Patent No. US6532164B2 (2001).

[4] O. J. Lee, V. S. Pribiag, P. M. Braganca, P. G. Gowtham, D. C. Ralph, and R. A. Buhrman, Appl. Phys. Lett. **95**, 012506 (2009).

[5] M. Marins de Castro, R. C. Sousa, S. Bandiera, C. Ducruet, A. Chavent, S. Auffret, C. Papusoi, I. L. Prejbeanu, C. Portemont, L. Vila, U. Ebels, B. Rodmacq, and B. Dieny, J. Appl. Phys. **111**, 07C912 (2012).

[6] A. D. Kent, B. Özyilmaz, and E. del Barco, Appl. Phys. Lett. **84**, 3897 (2004).

[7] H. Liu, D. Bedau, D. Backes, J. A. Katine, J. Langer, and A. D. Kent, Appl. Phys. Lett. **97**, 242510 (2010).

[8] D. Houssameddine, U. Ebels, B. Delaet, B. Rodmacq, I. Firastrau, F. Ponthenier, M. Brunet, C. Thirion, J.-P. Michel, L. Prejbeanu-Buda, M.-C. Cyrille, O. Redon, and B. Dieny, Nat. Mater. **6**, 441 (2007).

[9] J. Park, G. E. Rowlands, O. J. Lee, D. C. Ralph, and R. A. Buhrman, Appl. Phys. Lett. **105**, 102404 (2014).

[10] K. J. Lee, O. Redon, and B. Dieny, Appl. Phys. Lett. **86**, 022505 (2005).

[11] U. Ebels, D. Houssameddine, I. Firastrau, D. Gusakova, C. Thirion, B. Dieny, and L. D. Buda-Prejbeanu, Phys. Rev. B **78**, 024436 (2008).

[12] C. Papusoi, B. Delaet, B. Rodmacq, D. Houssameddine, J.-P. Michel, U. Ebels, R. C. Sousa, L. Buda-Prejbeanu, B. Dieny, and B. Delaët, Appl. Phys. Lett. **95**, 072506 (2009).

[13] J. C. Slonczewski, J. Magnet. Magnet. Mater. **159**, L1 (1996).

[14] J. Z. Sun, Phys. Rev. B **62**, 570 (2000).

[15] Z. Li and S. Zhang, Phys. Rev. B **68**, 024404 (2003).

[16] Z. Hou, Z. Zhang, J. Zhang, and Y. Liu, Appl. Phys. Lett. **99**, 222509 (2011).

[17] A. Mejdoubi, B. Lacoste, G. Prenat, and B. Dieny, Appl. Phys. Lett. **102**, 152413 (2013).

[18] J. Park, D. C. Ralph, and R. A. Buhrman, Appl. Phys. Lett. **103**, 252406 (2013).

[19] Y. B. Bazaliy, Phys. Rev. B **85**, 014431 (2012).

[20] B. Lacoste, L. D. Buda-Prejbeanu, U. Ebels, and B. Dieny, Phys. Rev. B **88**, 054425 (2013).